measurements in silicon and their empirical relation to electric field and temperature,'" *IEEE Trans. Electron Devices*, vol. ED-23, p. 1113, Sep. 1976.
[10] W. N. Grant, "Electron and hole ionization rates in epitaxial silicon at high electric fields," *Solid-State Electron.*, vol. 16, pp. 1189–1203, 1973.
[11] K. Board, "Thermal properties of annular and array geometry semiconductor devices on composite heat sinks," *Solid-State Electron.*, vol. 16, pp. 1315–1320, 1973.
[12] D. L. English, E. M. Nakaji, and R. S. Ying, "Improved performance of millimetre-wave IMPATT diodes on type-IIa diamond heat sinks," *Electron. Lett.*, vol. 12, pp. 675–676, Dec. 9, 1976.
[13] B. C. DeLoach, Jr., "Thin Skin IMPATT's," *IEEE Trans. Microwave Theory Tech.*, vol. MTT-18, pp. 72–74, Jan. 1970.
[14] A. I. Stoller, R. F. Speers, and S. Opresko, "A new technique for etch thinning silicon wafers," *RCA Rev.*, vol. 31, pp 265–271, June 1970.
[15] T. T. Fong, K. P. Weller, and D. L. English, "Circuit characterization of *V*-band IMPATT oscillators and amplifiers," *IEEE Trans. Microwave Theory Tech.*, vol. MTT-24, pp. 752–758, Nov. 1976.
[16] C. Chao, R. L. Bernick, E. M. Nakaji, R. S. Ying, K. P. Weller, and D. H. Lee, "*Y*-band (170–260 GHz) tunable CW IMPATT diode oscillators," *IEEE Trans. Microwave Theory Tech.*, vol. MTT-25, pp. 985–991, Dec. 1977.
[17] F. Sellberg, P. Weissglas, and G. Andersson, "A study of failure mechanisms in silicon IMPATT diodes," *IEEE Trans. Electron Devices*, vol. ED-25, pp. 742–746, June 1978.
[18] N. B. Kramer, "Millimeter wave semiconductor devices," *IEEE Trans. Microwave Theory Tech.*, vol. MTT-24, pp. 685–693, Nov. 1976.
[19] Y. Hirachi, T. Nakagami, Y. Toyama, and Y. Fukukawa, "High-power 50-GHz double-drift-region IMPATT oscillators with improved bias circuits for eliminating low frequency instabilities," *IEEE Trans. Microwave Theory Tech.*, vol. MTT-24, pp. 731–737, Nov. 1976.
[20] N. W. Cox, G. N. Hill, J. W. Amos, and C. T. Rucker, "Series interconnection of six TRAPATT devices on a diamond substrate," in *1976 IEEE Int. Microwave Symp. Dig.*, pp. 45–47.
[21] F. J. Bayuk and J. E. Raue, "*Ka*-band solid state power amplifier," in *1977 IEEE Int. Microwave Symp. Dig.*, pp. 29–31.

Millimeter-Wave Pulsed IMPATT Sources

T. T. FONG, MEMBER, IEEE, AND H. J. KUNO, FELLOW, IEEE

Invited Paper

***Abstract*—High-power millimeter-wave pulsed IMPATT sources have found a variety of applications as solid-state transmitters in radar applications. These applications have been greatly enhanced by the rapidly advancing millimeter-wave technology of which the high-power pulsed IMPATT source is a key element. In this paper the unique IMPATT properties which affect the oscillator spectral purity and coherency are reviewed. Some key considerations for the device design and system applications of the pulsed oscillators are discussed along with the state of the art, recent progress, and future trend.**

I. Introduction

AFTER A LONG, slow start, millimeter-wave systems development has been recently increasing at a rapid rate. A wide range of systems are now under development. Examples are tracking radar, missile seekers, radiometers, and short range communications. Millimeter-wave systems offer many advantages over both microwave systems and electrooptical systems. In comparison with microwave systems, millimeter-wave systems offer smaller size, lighter weight, improved accuracy, greater resolution, and smaller antenna size. Furthermore, in comparison with electrooptical or infrared systems, millimeter-wave systems provide greatly improved penetration through cloud, smoke, and dust. Most of the current activities for millimeter-wave systems are centered around 35 and 94 GHz, where atmospheric attenuation is relatively low. Development activities in the 140-GHz range, which is the next low atmospheric attenuation window, is now underway. The exploratory work now extends to a frequency as high as 240 GHz.

A key element in many millimeter-wave systems is the solid-state pulsed sources. These sources, because of their small size, light weight, and low voltage power supply requirements, are now finding applications as transmitters in many radar systems. In this paper, the state-of-the-art performance of millimeter-wave pulsed IMPATT oscillators is reviewed with in-depth discussion of the recent development and trend. Design and system application considerations that are unique to pulsed IMPATT oscillators are discussed. Design considerations for both diode and circuit, such as the strong temperature dependence of the diode impedance which results in frequency chirp during pulse, are covered. Methods for controlling the frequency chirp characteristics, phase and injection locking characteristics, and noise performance of transmitters

Manuscript received June 16, 1978; revised November 29, 1978.

T. T. Fong is with the Hughes Aircraft Company, Electron Dynamics Division, Torrance, CA 90509.

H. J. Kuno is with the Hughes Aircraft Company, Solid-State Subsystems Department, Torrance, CA 90509.

0018-9480/79/0500-0492$00.75 ©1979 IEEE

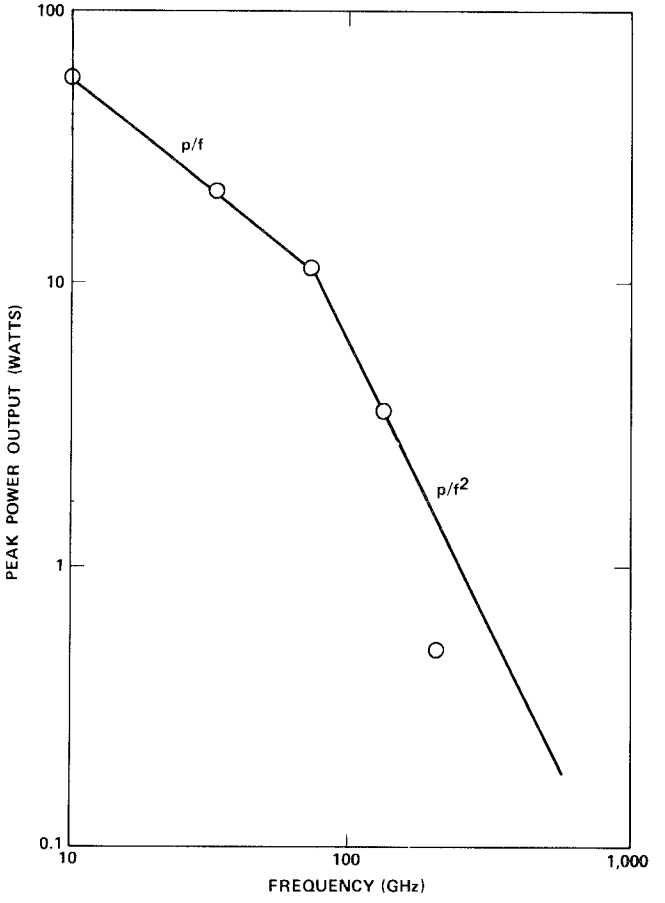

Fig. 1. State-of-the-art peak power output as a function of frequency for silicon double-drift IMPATT diode obtained with 100-ns pulsewidth and 50-kHz repetition rate.

developed for coherent radar systems are presented with an emphasis on the 94-GHz oscillators.

II. Diode Performance

Since the initial results [1]–[3] achieved with pulsed IMPATT oscillators in 1975 (10-W peak output power at 35 GHz and 1-W peak power at 94 GHz), the quest for higher peak power in silicon double-drift diodes for millimeter waves has continued with astonishing success. The progress has been measured at a 3-dB power increase per year rate in the past several years. To date, peak power outputs of 23 W at 35 GHz [4], 15 W at 94 GHz [5], and 3 W at 140 GHz [6] have been achieved. A typical pulsewidth of 100 ns and a pulse repetition rate of 50 kHz were used in these measurements. For most of the millimeter-wave radars, only short pulsewidth is of interest. The discussion in this paper is, therefore, focused on the short pulse applications.

To calibrate the present capability of millimeter-wave pulsed IMPATT oscillators, Fig. 1 shows the peak power output as a function of frequency for a single-diode oscillator. Below 100 GHz, the power reduction as a function of frequency follows the $1/f$ characteristic, indicating that the device power is limited by thermal constraints. Beyond 100 GHz, the power reduction follows the $1/f^2$ characteristic, indicating that the device is limited by device-circuit impedance matching. In practice, the pulsed oscillator must be constructed to operate in a range of environmental conditions. Power reduction must be allowed for isolator loss, temperature stabilization, and adjustment for specific frequency characteristics of the oscillator. Typically, a power reduction of 1–2 dB is experienced in an actual transmitter from the diode power output.

III. Diode and Circuit Designs

The pulsed double-drift IMPATT diodes are generally fabricated using silicon multiple epitaxy technique by first growing an n-layer on top of the n^{++}-substrate, followed by a p-layer growth and a shallow boron diffusion of 0.15 μm in depth. Ion implantation process is also used, specifically for high frequency diodes ($f > 140$ GHz). The silicon wafer is then metallized on both sides. Photolithography is subsequently used in defining and etching circular mesa diodes. An individual diode was then thermal compression bonded to a gold-plated copper disk. The diode processing is completed by packaging the IMPATT diode in a small ceramic (or quartz) ring, followed by ribbon bonding and capping. The scaled miniature package is designed for easy handling in RF evaluation as well as proper RF parasitics for impedance matching to the circuit. A miniature quartz ring diode package, which is used for operation 40–140 GHz, is shown in Fig. 2.

For short pulse double-drift IMPATT diodes, the primary design consideration is the impedance-frequency characteristic of the diode as a function of current density. Because IMPATT operation is strongly current dependent, the frequency for peak negative conductance is a function of the operating current. As current density increases, the optimum frequency increases and so does the diode output power. For CW diodes the maximum current density is limited thermally, but for pulsed diodes this limit is extended many times depending on the pulsewidth and duty factor. For extremely narrow pulsewidths and low duty operation, the diode is no longer thermally limited. The current density can be further extended until space-charge effects cause power saturation and efficiency reduction.

To properly design a pulsed diode, it is necessary to predetermine the operating current density. However, the operating current density is also intimately dependent on several other factors, such as pulsewidth, duty factor, power output, and device impedance. The choice of an optimum current density must, therefore, be derived from certain tradeoffs and the simultaneous optimization of a set of parameters. For a given optimum current density and a maximum operating junction temperature, the small-signal device admittance can be calculated for a given doping concentration. Strictly speaking, optimum diode design requires knowledge of the large-signal characteristics of the device, which in turn is strongly depen-

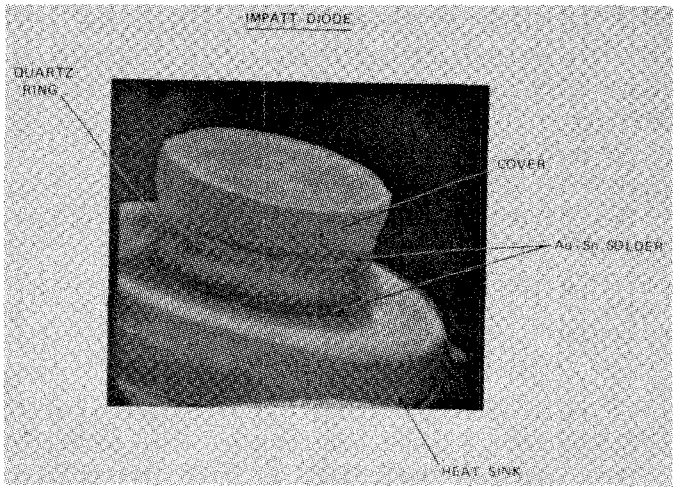

Fig. 2. A miniature quartz ring package designed for millimeter-wave pulsed IMPATT operation.

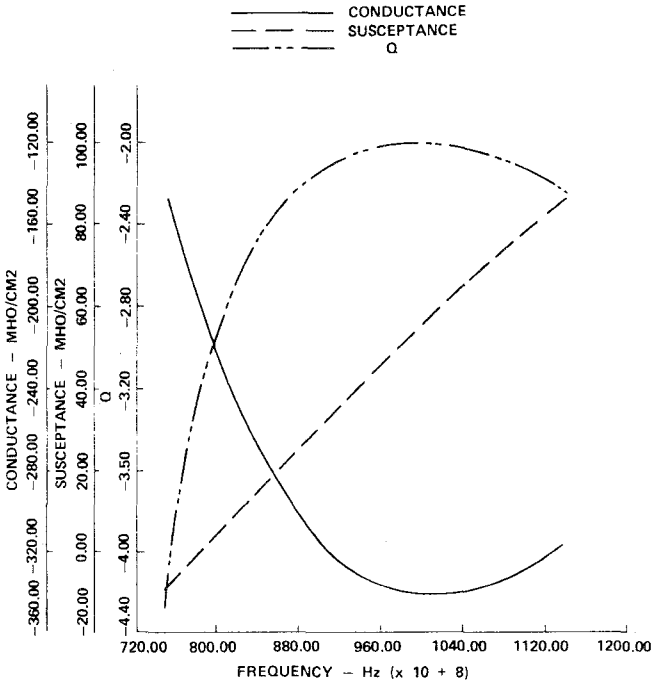

Fig. 3. Small-signal admittance as a function of frequency for a W-band pulsed silicon double-drift IMPATT diode. $N_A = N_D = 1.3 \times 10^{17}/\text{cm}^3$, $J = 60\,000$ A/cm^2.

dent on the circuit parameters. Since an exact analysis and accurate prediction of the circuit response is quite difficult to achieve in millimeter waves, the diode design generally is based on small-signal simultation to achieve a first-order diode design. Further optimization on the diode design is achieved by actual RF testing of the diode in a standard test circuit. The small-signal device admittance is obtained from a computer simulation based on the analysis of Misawa [7]. The analysis is quite general and includes the space-charge and temperature effects. By properly selecting the diode parameters, accurate small-signal device characteristics can be obtained. Fig. 3 shows an example of the diode admittance calculated based on the small-signal analysis. The diode was designed for

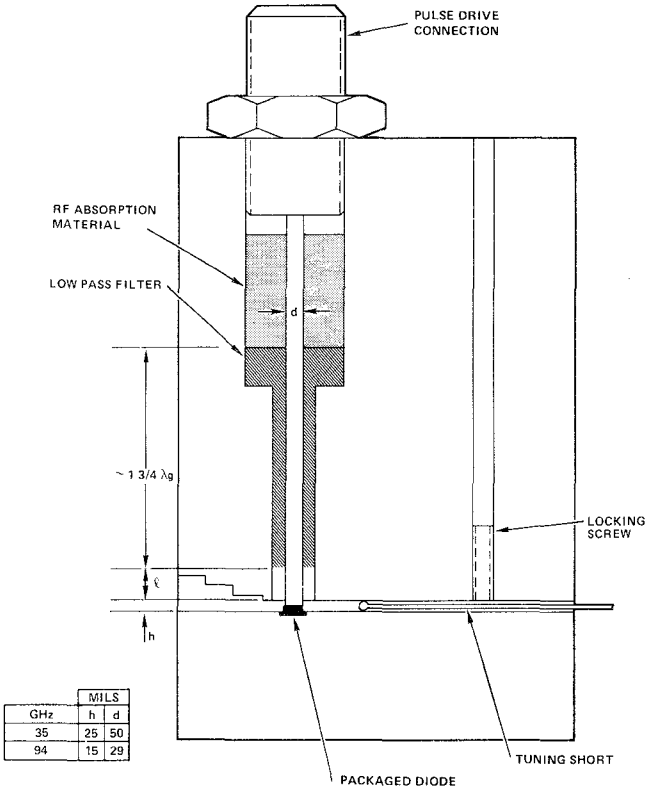

Fig. 4. A typical reduced height waveguide circuit for millimeter-wave pulsed IMPATT oscillator.

W-band operation, with $N_A = N_D = 1.3 \times 10^{17}$ cm^{-3}, $J = 6 \times 10^4$ A/cm^2, and operating peak temperature $T = 200$°C. The small-signal device admittance as shown in Fig. 3 is also useful as a starting point for circuit design.

Most of the pulsed oscillator results have been achieved in a reduced height waveguide. The cross section of the oscillator circuit is shown in Fig. 4. The diode is mounted on the bottom of the waveguide floor, and the bias is provided through a capacitive low-pass filter, which also serves as the feedthrough for the bias p-i-n to contact the diode package. A tuning short is provided behind the diode to obtain proper frequency and maximum power output. The circuit design is achieved again using computer simulation. For the simple reduced height waveguide circuit as shown in Fig. 3, an equivalent circuit model can be deduced based on approximate solutions to the boundary value problem pertaining to the circuit geometry [8]. Using the equivalent circuit model and the small-signal admittance of the diode, certain basic characteristics of the oscillator can be predicted. As an example, the device admittance shown in Fig. 3 may be replotted for the impedance as a function of frequency for a diode with a junction diameter of 100 μm. The circuit impedance presented to the diode for a reduced height waveguide as a function of tuning short position (waveguide height = 375 μm) can also be generated based on the equivalent circuit model as given in [8]. The intersection of the device reactance with circuit reactance determines the oscillator frequency, provided the negative resistance of the device is greater than the circuit load resistance at this point. It is seen in Fig. 5, for example, an oscillating

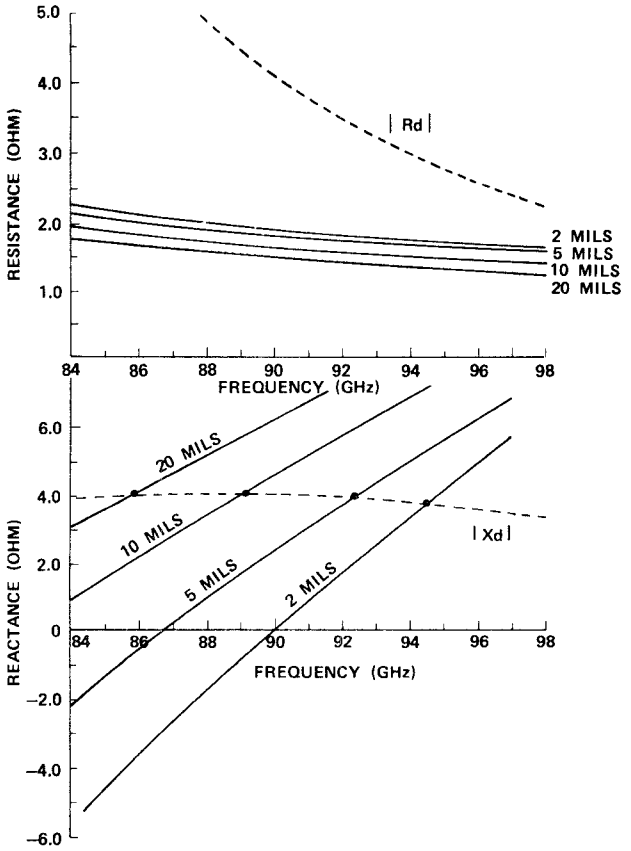

Fig. 5. Diode and circuit impedances calculated as a function of frequency for a W-band pulsed IMPATT oscillator.

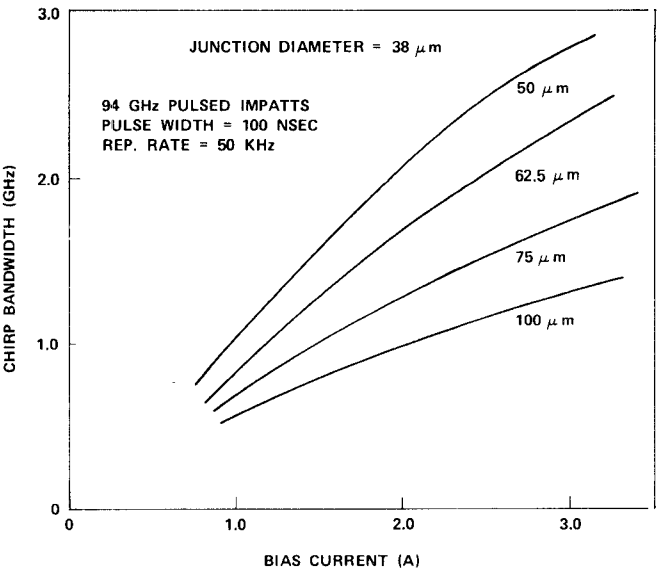

Fig. 6. Typical chirp bandwidth as a function of bias current for several diode junction diameters. Pulsewidth = 100 ns; repetition rate = 50 kHz.

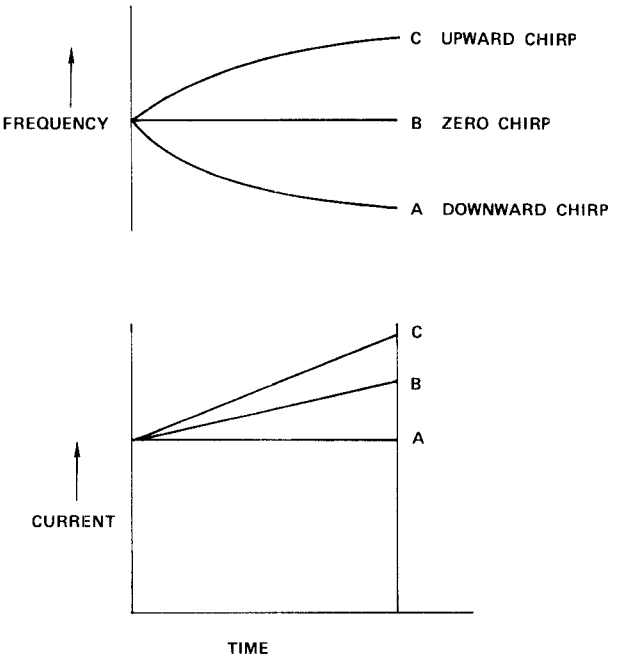

Fig. 7. Frequency chirp characteristics of a double-drift IMPATT diode responding to a current ramp.

frequency at 92.5 GHz is obtained for a short position of 125 μm from the bias post. This agrees closely with the actual measurements.

IV. Frequency and Temperature Characteristics of Pulsed Oscillators

A unique property of the pulsed IMPATT oscillator is the frequency chirp during the bias pulse. This effect is a direct consequence of the IMPATT junction temperature variation during pulse, which results in diode impedance change. For a flat current pulse, the diode junction is at a low temperature at the beginning of the pulse and gradually heats up with its thermal time constant. This temperature variation depends on current density, junction area, and thermal resistance. As the diode heats up during the pulse, the device impedance changes accordingly. In a fixed-tuned circuit, the oscillation frequency, therefore, varies according to the junction temperature change. The faster the diode heats up (a large transient thermal resistance), the greater the rate of chirp. A larger temperature excursion also leads to a greater amount of chirp. A typical measured chirp characteristic of 94-GHz pulsed double-drift IMPATT diode is plotted as a function of bias current for four diode junction diameters in Fig. 6. It is seen that, for a given bias current pulse, the chirp frequency (Δf) decreases with increasing junction diameter. This is due to the increase in the diode thermal time constant with the increasing junction diameter. For a fixed diode diameter, the chirp frequency increases with increasing bias current.

Since the diode impedance is also dependent on bias current, the amount of frequency chirp and rate of chirp can be controlled by the current pulse waveform. The frequency variation caused by the thermal effect can, therefore, be compensated by changing the operating current density. The method is illustrated in Fig. 7. For a flat current pulse, the oscillator frequency decreases (i.e., downward chirps). By providing an upward ramp on the current pulse, the amount of chirp can be decreased. A continuous increase in ramp slope will reach a point

where the thermal and current effects cancel each other and little chirp is present. Further increase in the ramp slope beyond this point will cause frequency to chirp upward. Thus by controlling the current waveform, the frequency chirp characteristics can be controlled.

The thermal properties as well as other parameters such as the doping profile and bias current density of the pulsed diode control the frequency characteristics of the pulsed IMPATT oscillator. The transient thermal characteristics of the diode deserve some discussions. Consider now the case of a uniform heat source with radius R on a semi-infinite heat sink of thermal conductivity K and thermal diffusivity α as shown in Fig. 7. The diode is under a periodic heating and cooling cycle caused by the bias pulses. It can be shown that the transient thermal resistance related to the maximum temperature at the center of the diode and at the end of a heating cycle is given by [9], [10]

$$\theta = \frac{2}{\pi RK} + \frac{d^{1/2}(\alpha t_1)^{1/2}}{\pi R^2 K}\left\{\frac{2}{(\pi d)^{1/2}}(1-e^{-R^2/4\alpha t_1}) - \frac{R}{(\alpha t_2)^{1/2}} + I + \frac{R}{d^{1/2}(\alpha t_1)^{1/2}}\operatorname{erfc}\left[\frac{R}{2(\alpha t_1)^{1/2}}\right]\right\} \quad (1)$$

where

$$I = \frac{2}{\pi d} \cdot \int_0^\infty \frac{e^{-dx^2}\{e^{-(1-d)x^2} - e^{-x^2}\}\{1-\cos\left[Rx^2(\alpha t_2)^{1/2}\right]\}}{x^2(1-e^{-x^2})}\,dx$$

and $d = t_1/t_2$ is the duty factor. The first term is a dc term proportional to the CW thermal resistance; the remainder of the terms consist of a dc contribution as well as an ac contribution following the heat pulse. For copper $K = 3.96$ W/cm°C and $\alpha = 1.14$ cm^2/s. Using these values, the transient spreading thermal resistance of a copper heat sink can be calculated using a computer. Fig. 8 presents the calculated transient thermal resistances of a pulsed IMPATT diode on copper heat sinks under a typical operational condition of 0.5-percent duty factor as a function of pulsewidth for four diode radii.

In an actual diode, the heat generation is confined mostly to the active layer close to the diode junction. Since the junction for the double-drift diode is formed by a multiple epitaxy process with the diode junction located at a distance from the heat sink, the silicon layer also contributes to the resistance of heat flow. For typical W-band diodes, this layer is approximately 0.4 μm thick with a diameter of 75–125 μm, its thermal mass is small, and so is the thermal time constant in comparison with the contributions of the heat sink. For all practical purposes, at the pulsewidths of interest, the thermal resistance contribution from this layer approaches its CW value. We can, therefore, approximate the thermal resistance caused by the silicon layer by

$$\theta_{Si} = \frac{t}{\pi R^2 K_{Si}} \quad (2)$$

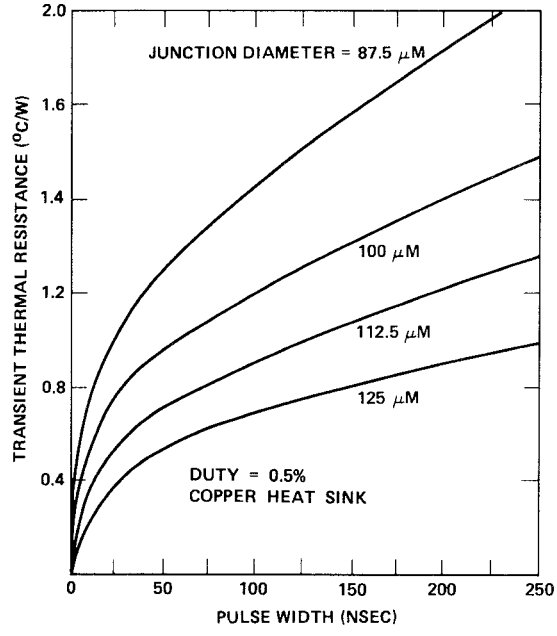

Fig. 8. Transient thermal resistance of a typical W-band pulsed IMPATT diode plotted as a function of pulsewidth for several diode junction diameters.

where t is the thickness of the silicon layer and K_{Si} is the thermal conductivity of silicon. For most homing and tracking radar applications, narrow pulsewidth is generally required to handle the target information at the close-in range. The normal pulsewidth requirement is typically less than 100 ns with a repetition rate less than 50 kHz. The total thermal resistance of an IMPATT diode including the transient thermal spreading resistance and the silicon layer contribution can be calculated using (1) and (2).

Given the input bias power, this thermal resistance defines the maximum junction temperature rise at the end of a heating cycle. For low duty operation, the "off" period is much longer than the "on" period. At the beginning of each heating cycle, the diode junction temperature is essentially at ambient temperature. Thus the temperature change during pulse is approximately equal to the maximum junction temperature rise.

V. Modulator for the Pulsed Sources

An important item in the development of highly stable, high power pulsed IMPATT oscillators is the pulse modulator. The pulse modulator must provide highly stable, fast rise-time current pulses up to 10 A with very small jitter. The modulator must also provide proper adjustment for current ramping, preferably with controls on both current magnitude and slope over small segments of the current pulse. The magnitude of chirp bandwidth and the linearity of the chirp can, therefore, be tailored for a specific application.

The block diagram of a modulator developed for 100–400-ns pulsewidth, low PRF, chirped millimeter-wave IMPATT oscillators is shown in Fig. 9. The modulator circuit consists basically of a dc resonance charged, SCR dis-

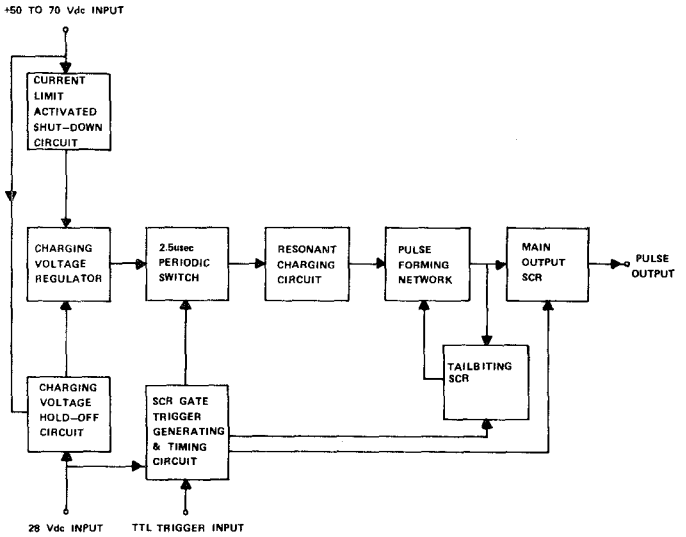

Fig. 9. Block diagram of a modulator designed for millimeter-wave pulsed IMPATT operation.

charged pulse-forming network. A tailbiting SCR shorts pulse-forming network (PFN) at the end of the desired pulse time so that a short fall time is obtained from the relatively slow PFN. The 2.5-μs periodic switch turns off the charging voltage regulator after each pulse so that the SCR's have time to recover before the PFN starts charging again.

This type of modulator is nearly ideal for low duty, high peak-power IMPATT oscillators because of the fast switching, high current capabilities of the SCR's. The PFN can be trimmed by means of terminal mounted capacitors and tunable inductors so that the pulse current waveform can be shaped to obtain the desired frequency chirp. Pulse current ramps up to 100 percent either up or down can be obtained. The modulator also has an auxiliary circuitry for prevention of SCR latchup and for short-circuit protection. RF pulse rise and fall times of 5 ns have been obtained with millimeter-wave IMPATT diodes pulsed with this modulator.

VI. Noncoherent Pulsed Oscillators

A class of millimeter-wave radar has been developed which utilizes chirped IMPATT oscillators as transmitters. In this type of radar, the pulsed IMPATT oscillator typically has a chirp bandwidth of 500–1000 MHz. The receiver must have the corresponding bandwidth. The signal reflected back from the target is integrated over the bandwidth that results in an improved background clutter-to-signal ratio. The pulsed IMPATT oscillator is ideal for this application because of its natural chirp as a result of diode heating during the bias pulse. With a properly designed modulator to provide a current ramp in the bias current pulse, the chirp bandwidth and linearity of chirp can be controlled to meet a specific requirement.

Fig. 10 shows a pulsed silicon IMPATT oscillator including an integrated isolator and modulator at 94 GHz. Typical peak power output of 10 W at 100-ns pulsewidth and 50-kHz repetition rate is achieved reproducibly at 94

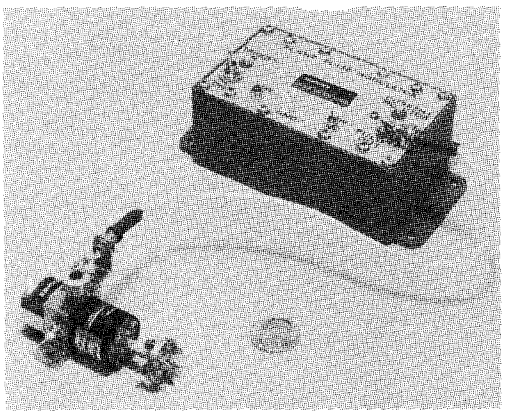

Fig. 10. A 94-GHz pulsed IMPATT oscillator shown with integrated isolator and modulator.

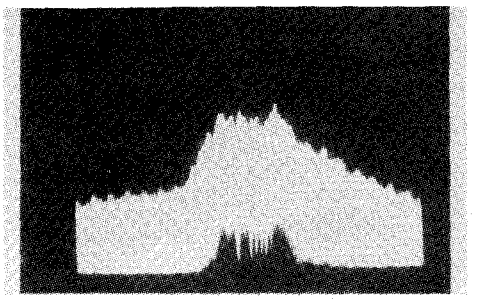

Fig. 11. Chirp bandwidth of a 94-GHz pulsed IMPATT oscillator as displayed on spectrum analyzer. Horizontal: 100 MHz/div.; vertical: 10 dB/div.

GHz. This type of oscillator has been used as a transmitter in prototype radars which produced excellent results. A typical spectral output of a chirped oscillator at 94 GHz is shown in Fig. 11. The output was obtained by mixing the output from the pulse oscillator with a CW local oscillator and a single-ended mixer to derive an IF output at 2 GHz. The IF spectral output is then displayed using a spectrum analyzer. As shown in Fig. 11, the pulsed source was adjusted for a chirp bandwidth of 500 MHz with a high degree of linearity as evidenced by the flat response of the spectral output. The relative gradual decrease in power at the high end of the IF bandwidth is caused by the finite fall time of the modulator. With an improved rise/fall time in the bias current waveform to reduce the unwanted frequency components, a nearly square-wave spectral output can be achieved.

VII. Coherent Pulsed Oscillators

For a Doppler radar system, the FM noise of an oscillator close to carrier must be kept low to ensure high receiver sensitivity. Equally important is the pulse-to-pulse phase coherency of the pulsed oscillator. A free running pulsed IMPATT oscillator with frequency chirp during pulse is no longer useful for this application. Injection or phase locking with a highly stable reference oscillator is necessary to achieve frequency and phase coherency in a pulsed IMPATT oscillator.

Coherent transmitters phase locked to a crystal oscillator reference signal have been developed in which both

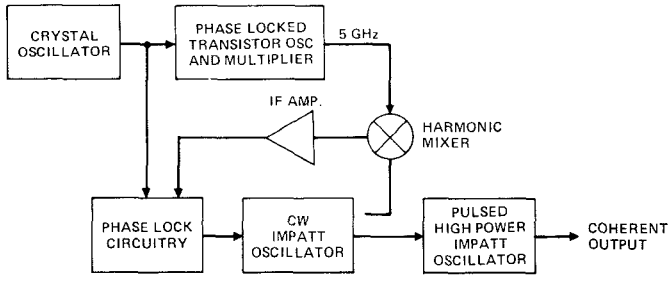

Fig. 12. Block diagram of a coherent 94-GHz pulsed transmitter using both phase- and injection-locking techniques.

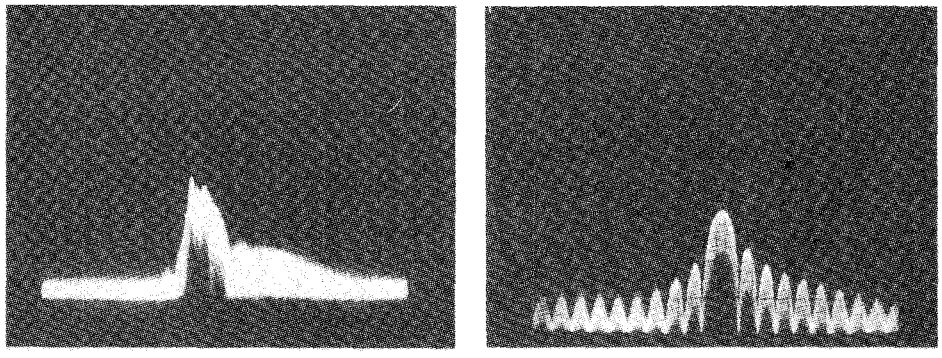

Fig. 13. Spectral output for 1 94-GHz pulsed IMPATT oscillator: (a) free running, (b) injection locked with a stable source. Horizontal: 100 MHz/div.; vertical: 10 dB/div.

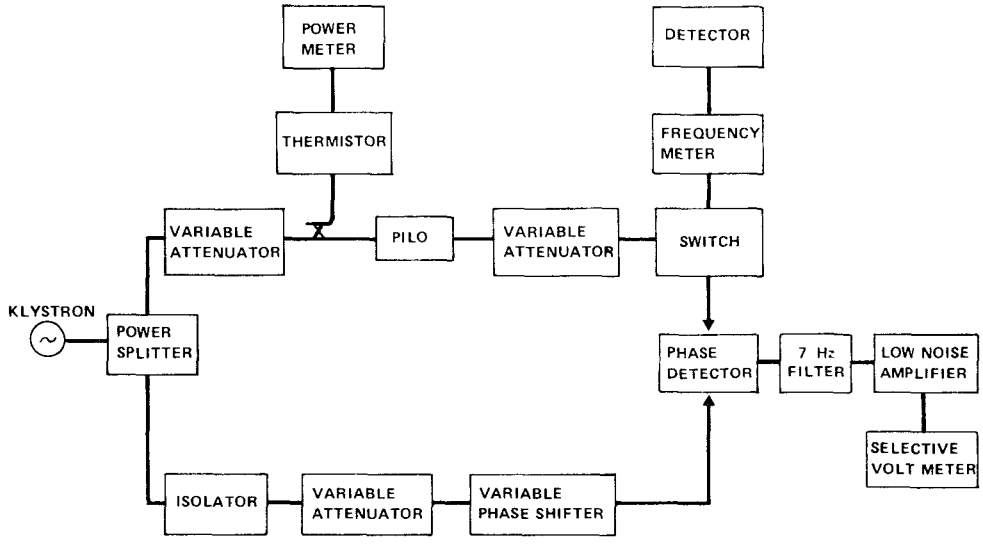

Fig. 14. The phase bridge test setup for measurements on FM noise and pulse-to-pulse coherency of a millimeter-wave pulsed IMPATT oscillator.

phase-locking and injection-locking techniques are used. The FM noise of the coherent pulsed oscillator has been evaluated extensively. Based on the experimental results accumulated, it can be concluded that millimeter-wave pulsed IMPATT oscillators can be used as coherent transmitters. In order to achieve low FM noise from the pulsed coherent oscillator, care must be exercised to minimize the free running chirp bandwidth by controling the bias current waveform. The minimum chirp bandwidth (on the order of 100 MHz) ensures that the locking bandwidth is greater than the chirp bandwidth for a given gain so that the system will stay locked over the operating environment conditions. The block diagram of a three-stage coherent transmitter at 94 GHz is shown in Fig. 12. In this transmitter, a Gunn oscillator is phase locked to a highly stable crystal oscillator. The stable output from the Gunn oscillator ($P_0 = 5$ mW) was used for injection locking a CW IMPATT oscillator. The output of the CW IMPATT

oscillator was then used to injection lock the pulse oscillator with 5-W peak output power operated with 100-ns pulsewidth at 50-kHz repetition rate.

As a first-order indication, the coherency of the pulsed oscillator can be characterized with a spectrum analyzer. Fig. 13 shows the frequency spectrum of the pulsed oscillator as a free running oscillator (Fig. 13(a)) and injection-locked oscillator (Fig. 13(b)). The pulsed spectrum was obtained using a spectrum analyzer after the pulsed signal is down-converted to an IF output at 2 GHz. It is seen that the coherency of the pulsed IMPATT oscillator indeed can be substantially improved by means of injection locking from a stable source.

The FM noise close to carrier which is also a measure of the pulse-to-pulse coherency may be evaluated by means of a phase bridge. The phase bridge measurement setup is shown in Fig. 14. When the bridge is balanced for minimum phase detector output, the noise contributed by the input signal is cancelled by the bridge. The noise measured by the phase bridge output, therefore, represents the additive noise contribution of the pulsed oscillator. The signal-to-noise ratio of the pulsed oscillator can be obtained by maximizing the phase detector output which is then compared with the noise measured in the balanced state of the bridge. The peak-to-valley ratio, measured by a wave analyzer, is plotted as a function of frequency from carrier as shown in Fig. 15. The peaks represent the signal strength of the pulsed oscillator occurring at the pulsed repetition frequency. The valleys represent the FM noise caused by the pulsed IMPATT oscillator and pulse-to-pulse incoherency. The peak-to-valley ratio, therefore, is a measure of signal-to-noise ratio of the pulsed oscillator. As seen in Fig. 15, at 20 kHz away from carrier, a signal-to-noise ratio of 60 dB per 1-kHz bandwidth is achieved with the injection-locked pulsed IMPATT oscillator at 94 GHz, which is a level sufficiently low for many doppler radar applications. The oscillator was operated at 100-ns pulsewidth and 50-kHz repetition rate with 5-W peak power output.

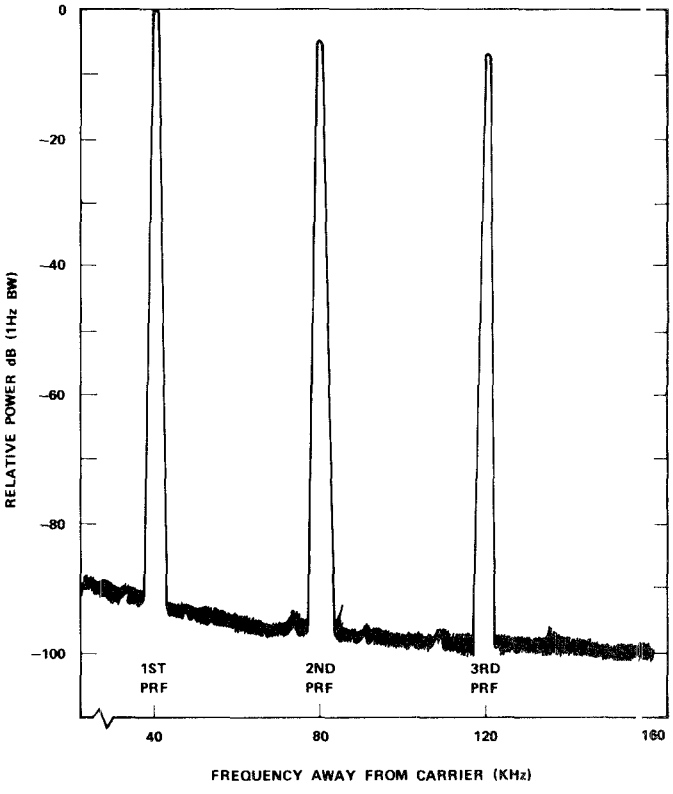

Fig. 15. Signal-to-noise ratio of a 94-GHz pulsed IMPATT oscillator measured with the phase bridge shown in Fig. 14.

VIII. Conclusion

The state of the art of millimeter-wave pulsed IMPATT oscillators is reviewed in this paper. Design considerations, means of controlling the frequency chirp, and methods of achieving highly coherent output spectrum are discussed including phase- and injection-locking techniques. The solid-state pulsed oscillators can now produce sufficient peak power output for many short-range radar applications. Techniques have also been developed to control the oscillator operating parameters for many millimeter-wave systems currently under development. It is believed with further development in the diode and circuit, high power pulsed IMPATT oscillators will find a wide range of applications in future radar systems.

Although the powers available from a solid-state device are still considerably lower than a vacuum tube device, techniques to combine a number of individual millimeter-wave IMPATT diodes to achieve higher power are not being pursued. It is reasonable to project that, with the technology advancing at the current pace, peak powers on the order of 200–500 W will be achieved at 35 and 94 GHz in the next three to five years. Perhaps, with the increased power, millimeter-wave solid-state transmitters will also be utilized in longer range applications, such as imaging radars for RPV's and surface-to-air/air-to-air missile guidance systems, where the detection of fast approaching, small cross-sectional targets is essential.

References

[1] R. S. Ying *et al.*, "Millimeter-wave pulsed IMPATT oscillators," *IEEE J. Solid-State Circuits*, vol. SC-11, pp. 279–285, Apr. 1976.
[2] C. Chao *et al.*, "Pulsed IMPATT diode oscillators above 200 GHz," presented at the 1977 IEEE Int. Solid-State Circuits Conf., Philadelphia, PA, Feb. 1977.
[3] T. T. Fong, W. R. Lane, H. J. Kuno, and N. B. Kramer, "High power W-band pulsed IMPATT oscillators," in *1977 IEEE Int. Microwave Symp. Dig.*, San Diego, CA, pp. 20–21, 1977.
[4] M. Simonutti, D. L. English, and E. M. Nakaji, "High power Ka-band pulsed oscillators," to be published.
[5] K. Chang, C. Sun, D. L. English, and E. M. Nakaji, "High power W-band pulsed IMPATT oscillators," to be published.
[6] M. Ngan and E. M. Nakaji, "140 GHz pulsed IMPATT oscillators," to be published.
[7] T. Misawa, "Negative resistance in p–n junction under avalanche breakdown conditions, Parts I and II," *IEEE Trans. Electron Devices*, vol. ED-13, pp. 137–151, Jan. 1966.
[8] T. T. Fong, K. P. Weller, and D. L. English, "Circuit characterization of V-band IMPATT oscillators and amplifiers," *IEEE Trans. Microwave Theory Tech.*, vol. MTT 24, pp. 752–758, Nov. 1976.
[9] J. C. Jaeger, "Pulsed surface heating of semi-infinite solids," *Australian J. Quarterly Mathematics*, vol. XI, pp. 123–137, 1953.
[10] G. Gibbons, "Transient temperature response of an avalanche diode," *Solid State Electron.*, vol. 13, pp. 799–806, Aug. 1969.